Photon Acceleration in a Flying Focus

A. J. Howard, D. Turnbull, A. S. Davies, P. Franke, D. H. Froula, and J. P. Palastro
University of Rochester, Laboratory for Laser Energetics, Rochester 14623, New York, USA

(Received 30 April 2019; revised manuscript received 3 July 2019; published 20 September 2019)

A high-intensity laser pulse propagating through a medium triggers an ionization front that can accelerate and frequency upshift the photons of a second pulse. The maximum upshift is ultimately limited by the accelerated photons outpacing the ionization front or the ionizing pulse refracting from the plasma. Here, we apply the flying focus—a moving focal point resulting from a chirped laser pulse focused by a chromatic lens—to overcome these limitations. Theory and simulations demonstrate that the ionization front produced by a flying focus can frequency upshift an ultrashort optical pulse to the extreme ultraviolet over a centimeter of propagation. An analytic model of the upshift predicts that this scheme could be scaled to a novel tabletop source of spatially coherent x rays.

DOI: 10.1103/PhysRevLett.123.124801

A growing number of scientific fields rely critically on high-intensity, high-repetition rate sources of extreme ultraviolet (XUV) radiation (wavelengths <120 nm). These sources provide high-resolution imaging for high energy density physics and nanotechnology [1,2], fine-scale material ablation for nanomachining, spectrometry, and photolithography [3–5], and ultrafast pump-probe techniques for fundamental studies in atomic and molecular physics [6–8]. While XUV sources have historically been challenging to produce, methods including nonlinear frequency mixing [9], high harmonic generation [10,11], and XUV lasing or line emission in metal-vapor and noble-gas plasmas [5,12] have demonstrated promising results. Despite their successes, each of these methods introduces tradeoffs in terms of tunability, spatial coherence, divergence, or efficiency [5,9–12]. Photon acceleration offers an alternative method for tunable XUV production that could lessen or even eliminate these tradeoffs.

Photon acceleration refers to the frequency upshift of light in response to a refractive index that decreases in time [13,14]. In analogy to charged particle acceleration, an increase in photon energy, i.e., frequency, accompanies an increase in group velocity. In the context of an electromagnetic pulse, the leading phase fronts experience a higher index than adjacent, trailing phase fronts, which manifests as a local phase velocity that increases over the duration of the pulse. The trailing phase front, on account of its higher phase velocity, gradually catches up with the leading front, compressing the wave period. In a medium with normal dispersion, the resulting frequency upshift translates to an increase in the local group velocity.

Plasmas provide an ideal medium for photon acceleration: the refractive index depends on the density of free electrons, which can be rapidly increased or decreased over time through ionization and recombination or manipulated through electrostatic wave excitation. Specifically, a photon of frequency ω in an isotropic plasma experiences a refractive index $n(\omega)=(1-\omega_p^2/\omega^2)^{1/2}$, where $\omega_p=(e^2n_e/m\varepsilon_0)^{1/2}$ is the plasma frequency, n_e the free electron density, e the elementary charge, m the electron mass, and ε_0 the permittivity of free space. An increase in the electron density over time—for example by ionization—provides a decreasing refractive index that will accelerate the photons of a colocated pulse.

A prototypical scheme for photon acceleration involves propagating a witness pulse in an ionization front triggered by a copropagating drive pulse [15–21]. In spite of the impressive frequency shifts (>10×) predicted by theory and simulations [13–17,22–24], experiments in the optical regime have met with limited success (∼1.25×) [18,19,21,25] on account of diffraction and ionization refraction. Even if these could be remedied, a fundamental limitation to the upshift would remain. The drive pulse, and hence the ionization front, travels at a subluminal group velocity. As the witness pulse accelerates, it quickly outpaces the front, terminating the interaction.

In this Letter, we demonstrate, for the first time, a scheme for photon acceleration within a copropagating ionization front that shifts an optical pulse to the XUV. The scheme utilizes a novel photonic technique known as the *flying focus* [26,27] and a shaped gas target to overcome the aforementioned limitations [28–30]. The shaped gas target has a density profile that increases quadratically with radius [30]. When ionized, the profile provides a plasma waveguide that prevents the diffraction and refraction of the witness pulse regardless of its frequency [28,29]. An appropriately chirped drive pulse focused through a chromatic lens—or flying focus—exhibits an intensity peak that counterpropagates at the speed of light in vacuum c with respect to its group velocity [26,31,32]. This intensity peak triggers an ionization front traveling at c, which can

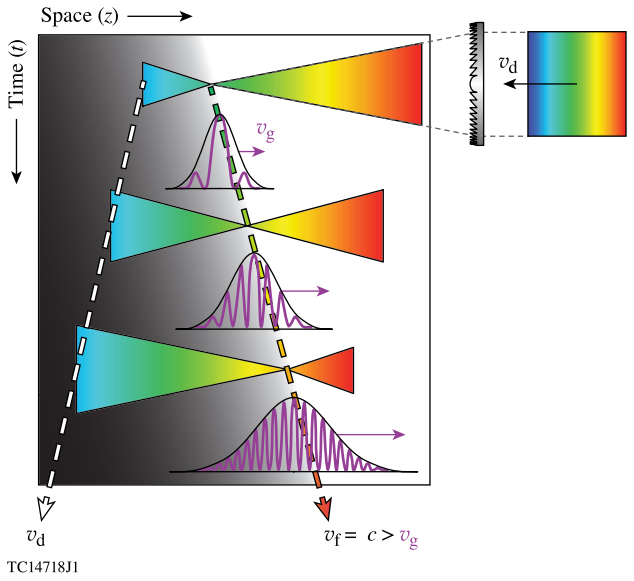

FIG. 1. A schematic demonstrating photon acceleration in the ionization front of a flying focus. A negatively chirped drive pulse propagating at its group velocity $v_d < 0$ forms a focus that counterpropagates at the velocity $v_f = c$, triggering an ionization front traveling at c. The resulting electron density is indicated by shading. A witness pulse (drawn in purple) copropagates with the ionization front at velocity v_g and continually upshifts in frequency.

continually accelerate the photons of a copropagating witness pulse without the possibility of dephasing. Counterpropagating the drive pulse with respect to the ionization front also mitigates ionization refraction, as the focus of the drive pulse only encounters un-ionized medium [31,32]. Furthermore, the interaction distance is solely determined by the flying focus parameters and can be extended long past the Rayleigh range of any single frequency component within the drive pulse.

A schematic is displayed in Fig. 1 for the case of a diffractive optic. The intensity peak of the drive pulse travels through the focal region $z_f = (\Delta\lambda/\lambda_c)f$ at the focal velocity, $v_f = (1 + v_d T/z_f)^{-1} v_d$, where λ_c is the central wavelength of the drive pulse, $\Delta\lambda/\lambda_c$ its fractional bandwidth, f the focal length of the diffractive optic at λ_c, $v_d = cn$ the group velocity, and T the stretched pulse duration.

The flying focus photon accelerator modeled here consists of two frequency-doubled Ti:sapphire pulses, i.e., the witness and drive pulses, and a shaped hydrogen gas target (see Table I for parameters). The self-consistent evolution of the drive pulse and the ionization of the gas target were simulated using a 2D+time cylindrically symmetric propagation code [31]. The gas target had a spatial profile defined by $n_g = n_{g0}(1 + r^2/R_g^2)$ for $r \le R_g$ and $n_g = 2n_{g0}$ for $r > R_g$. The flying focus drive pulse ionizes the gas target creating a plasma waveguide. Figure 2(a) shows an example at $z = 0.7$ cm, measured

TABLE I. Parameters chosen for the drive pulse and propagation medium. SG refers to Super-Gaussian order.

Drive pulse parameters	Value
Central wavelength	400 nm
Bandwidth	6 nm
Stretched duration	54 ps
Energy	5.6 J
Radial profile	SG 8
Spectral pulse shape	SG 10
Focal length	1.02 m
f number	14
Witness pulse parameters	
Duration (2nd moment)	87 fs
Medium parameters	
Species	H_2
Central density	8.8×10^{20} cm^{-3}
Radius	100 μm
Ionization energy	13.6 eV

from the start of the accelerator, plotted as a function of r and the moving frame coordinate $-\xi = z - ct$. A lineout at $-\xi = -25$ μm [demarcated by the dashed line in Fig. 2(a)] is displayed in Fig. 2(b). The profile readily satisfies the guiding condition: $n_e^{\max} - n_e^{\min} > 1/\pi r_e R_e^2$ where r_e is the classical electron radius and R_e the radial location of $n_e^{\max}$ [29]. With the guiding condition satisfied, the propagation of the witness pulse can be treated as one dimensional, analogous to light propagating in a fiber. To model the

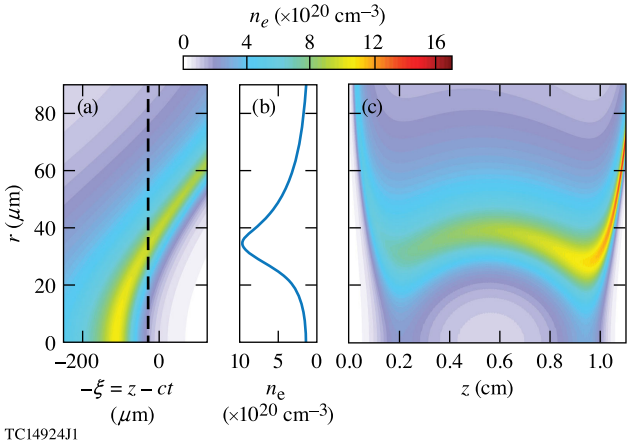

FIG. 2. Profiles of the plasma guiding structure created when the flying focus drive pulse ionizes the shaped gas target. (a) The transverse profile as a function of moving frame coordinate $-\xi = z - ct$ at $z = 0.7$ cm. (b) A line out corresponding to the dashed line in (a). (c) The guiding profile experienced by a typical photon within the witness pulse along the length of the accelerator (i.e., at each z, the transverse profile was extracted at the ξ location of the photon).

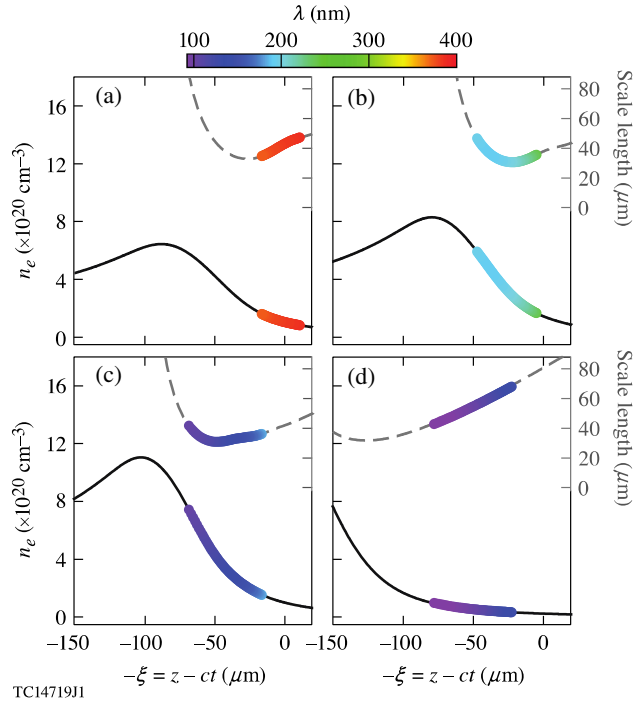

FIG. 3. A series of snapshots of an 87 fs witness pulse with an initial wavelength $\lambda = 400$ nm copropagating with a temporal gradient in the electron density. The snapshots are taken at propagation distances of (a) 0.1, (b) 0.3, (c) 0.8, and (d) 1.05 cm and plotted in the moving frame $-\xi = z - ct$. The pulse is modeled by photons initially spaced evenly in time over 87 fs. Each photon is represented by a circle colored to correspond to its vacuum wavelength (color bar). The electron density and scale length, $L = n_e/\partial_\xi n_e$, are shown as solid black and dashed gray lines, respectively.

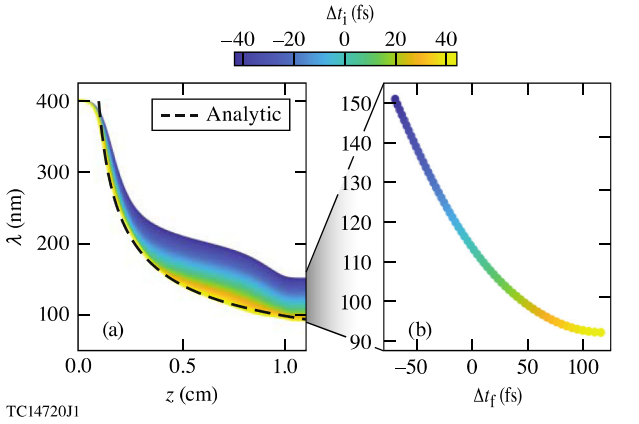

FIG. 4. (a) A plot of vacuum wavelength λ over propagation distance z for a pulse modeled by a series of photons evenly distributed over an input duration of 87 fs, each with a color corresponding to the initial temporal location within the pulse Δt_i (color bar). For comparison, the analytic case is plotted for the highest-frequency photon (dashed black line). (b) The distribution of wavelength over the final duration of the witness pulse Δt_f for the simulated case shown in (a).

witness pulse propagation, the on-axis electron density profile from the propagation simulation, as a function of propagation distance and time, was coupled to a 1D photon kinetics simulation [14].

Figure 3 shows results of the photon kinetics simulation demonstrating that the ionization front formed by the flying focus can upshift the frequency of an 87 fs witness pulse from the optical ($\lambda = 400$ nm) to the XUV ($\lambda = 92$ nm). The photons of the witness pulse enter the ionization front in Fig. 3(a), each with an initial vacuum wavelength of 400 nm. The photons continually upshift in frequency as they copropagate with a temporal gradient in electron density as seen in Figs. 3(b) and 3(c). After ~1 cm, the photons—now upshifted to a minimum vacuum wavelength of 92 nm—approach the end of the focal region, terminating their upshift. Figure 2(c) illustrates the plasma density profile experienced by a typical photon within the witness pulse at each point in interaction region: the photon sees a guiding profile over the entire length.

Figure 4 displays the evolution of the vacuum wavelength and the final dispersion of the pulse. The witness pulse acquires a broad bandwidth of 58 nm, but retains an ultrashort duration, ~190 fs. The dispersion, from 92 nm at the leading edge to 150 nm at the trailing edge, results from the unique inhomogeneity in the temporal gradient experienced by each photon along its path (see Fig. 3). The nonlinear inhomogeneity causes substantially less temporal stretching than an idealized linear gradient: ~190 fs compared to ~380 fs [15].

The initial rapid decrease in vacuum wavelength gradually slows due to the weakening plasma response, $n^2 - 1 = -\omega_p^2/\omega^2$. An analytic model, shown as the black dashed curve in Fig. 4(a), predicts this effect [15]. Assuming an electron density profile with a constant gradient moving at c, the vacuum wavelength evolves according to

$$\lambda(z) = \left(1 + \frac{\omega_{p0}^2}{\omega_0^2}\frac{z}{L_T}\right)^{-1/2}\lambda_0, \tag{1}$$

where λ_0 is the initial vacuum wavelength of a photon in the witness pulse, $\omega_0 = 2\pi c/\lambda_0$, and ω_{p0} is the value of the plasma frequency at $\xi = L_T$. The value of ω_{p0}^2/L_T used in Fig. 4(a) was averaged over the path of the highest-frequency photon.

Inspection of Eq. (1) reveals two paths to shorter wavelengths: increasing the interaction length or decreasing the scale length. The interaction length $z_f = (\Delta\lambda/\lambda_c)f$ can be extended by increasing the bandwidth of the drive pulse or the focal length, while the scale length can be decreased by shortening the effective duration of the flying focus intensity peak such that ionization occurs more rapidly.

Figure 5 illustrates the efficacy of this scheme compared to the prototypical photon accelerator. Without a flying

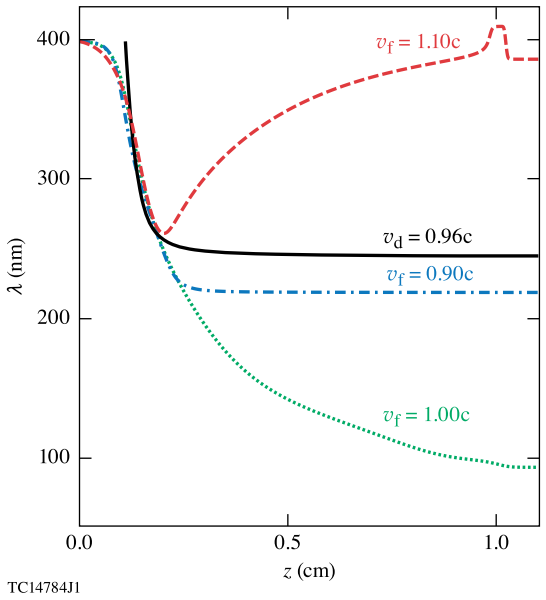

FIG. 5. A plot of minimum vacuum wavelength over propagation distance, displayed for four separate ionization front velocities. Drawn in a green dotted line is a reproduction of the simulated case in Fig. 4(a), with a flying focus focal velocity of $v_f = c$; in a red dashed line is a superluminal case in which $v_f = 1.1c$; in a blue dash-dotted line is a subluminal case in which $v_f = 0.9c$; in a black solid line is a case in which no flying focus is formed, and instead, the ionization front travels at the group velocity of the drive pulse $v_d = 0.96c$.

focus, the drive pulse *copropagates* with the witness pulse. To emulate this case, three generous simplifications are made in the simulation: First, it is assumed that a prototypical photon accelerator utilizes a guiding structure for the witness pulse. Second, ionization refraction of the drive pulse is ignored. Finally, the ionization front travels at a group velocity $v_d = 0.96c$—the group velocity corresponding to one third of the peak electron density. Even with these advantages, the prototypical photon accelerator only achieves a minimum vacuum wavelength of 245 nm (black solid curve), a fractional shift of ~1.6 compared to ~4.3 when using a flying focus. Additionally, when $v_f = c$, the wavelength could be further downshifted by extending z_f, whereas in the prototypical accelerator, no further frequency conversion is possible.

The parameters used for the examples above (see Table I) were chosen to represent current experimental capabilities. The drive and witness pulse bandwidths are consistent with a chirped pulse undergoing second harmonic generation in potassium dideuterium phosphate at an intensity below the damage threshold [33]. The focal length was chosen such that, when using 6 nm of bandwidth, the longitudinal focal region would be large enough ($z_f > 1$ cm) to ensure significant wavelength shifts, but small enough to remain computationally viable. After fixing the length of the focal region, the focal velocity was tuned by adjusting the chirp of the drive pulse. The blue dash-dotted and red dashed curves in Fig. 5 illustrate the consequences of tuning the chirp for too low or too high of a focal velocity, respectively. When too low, the witness pulse quickly outruns the ionization front; when too high, the ionization front outruns the witness pulse. In either case, the wavelength shift is reduced. Notably, the subluminal focal velocity still outperforms the prototypical accelerator.

A high-density gas was used to maximize the temporal gradient of the electron density. At a gas density of $8.8 \times 10^{20}\,\mathrm{cm}^{-3}$, it was found that 5.6 J of pulse energy yielded a near maximum electron density ($\sim 1.2 \times 10^{21}\,\mathrm{cm}^{-3}$), with further increases in energy providing diminishing returns. While more robust to ionization refraction than a traditional pulse, the flying focus began to undergo plasma refraction, preventing the peak intensity from (1) reaching the plasma and (2) providing a heat source to overcome cooling from impact ionization. With the high density and cooling, three-body recombination limited the maximum density. Nevertheless, the flying focus pulse created a sharp gradient over the entire focal region ~1 cm, a distance nearly 2 orders of magnitude greater than the Rayleigh range (~366 μm).

A full description of the propagation model for the drive pulse, including assumptions and the ionization model, can be found in Ref. [31]. Ultimately, the electron density profile is modified by field ionization, collisional ionization, and three-body recombination, while the temperature evolves through inverse Bremsstrahlung absorption and ionization cooling. The photon kinetics equations used to evolve the witness pulse are derived from the Eikonal approximation to the electromagnetic wave equation. To the lowest order, one finds the photon Hamiltonian $\omega = (\omega_p^2 + c^2 k_z^2)^{1/2}$, where k_z is the wave number parallel to the propagation axis, which provides equations of motion for refraction, the group velocity, and frequency conversion:

$$\frac{dk_z}{dz} = \frac{1}{2c^2 k_z}\left(\frac{\partial}{\partial \xi} - \frac{\partial}{\partial z}\right)\omega_p^2, \tag{2}$$

$$\frac{d\xi}{dz} = \frac{\omega}{ck_z} - 1, \tag{3}$$

$$\frac{d\omega}{dz} = \frac{1}{2ck_z}\frac{\partial \omega_p^2}{\partial \xi}. \tag{4}$$

At the next order, the Eikonal approximation yields the transport equation for the photon energy density:

$$\frac{\partial E_0^2}{\partial t} + \frac{\partial}{\partial z}(v_g E_0^2) = -\frac{1}{\omega}\frac{d\omega}{dt}E_0^2, \tag{5}$$

where E_0 is the electric field amplitude of the witness pulse. According to Eq. (5), the quantity $G = \omega E_0^2$ is conserved along a photon trajectory: as the witness pulse upshifts in frequency, it decreases in energy density, translating to a loss in photon number. Physically, the witness pulse loses energy

by imparting the electrons within the ionization front with a drift momentum as they are freed. Using Eq. (5), the simulated witness pulse exits the ionization front with approximately 25% of its initial energy after undergoing a frequency upshift by a factor of ~4.

To estimate the efficiency, consider a witness pulse with an intensity just below the photoionization threshold—an intensity low enough to ensure that the drive pulse accounts for nearly all of the photoionization and heating that sustains collisional ionization. The simulations show that the drive pulse creates an approximately 50 μm diameter ionization front. Using a square-pulse approximation, the witness pulse energy is estimated as $E_w = I_w A_w T_w$, where I_w is the witness pulse peak intensity ($\sim 1.0 \times 10^{14}$ W/cm^2), A_w the area of the ionization front (~ 2000 μm^2), and T_w the witness pulse duration (~87 fs), providing $E_w \sim 170$ μJ. For an input energy of 5.6 J and an output of 43 μJ in the XUV, the overall efficiency becomes roughly 10^{-5}. This analysis does not, however, take into account the efficiency of the frequency doubling process used to generate the pulses (~80% [33]). With an output of 43 μJ, this scheme compares favorably to plasma-based soft x-ray lasers and previous experiments of photon acceleration that demonstrated more modest wavelength shifts (from $\lambda = 620$ nm to 604 nm) [8,21].

A novel scheme for photon acceleration in a luminal ionization front has been shown to upshift optical photons to the XUV. By applying a shaped gas target and the recently demonstrated spatiotemporal technique, the "flying focus," the scheme eliminated the inherent limitations of a prototypical photon accelerator: refraction and diffraction of the witness and drive pulses and the outpacing of the front by the accelerated photons. By increasing the bandwidth of the drive pulse or the focal length, this scheme could be scaled to produce shorter vacuum wavelengths, representing a promising method for the production of spatially coherent x rays at the tabletop scale.

The authors would like to thank W. Knox, K. Qu, M. R. Edwards, and N. J. Fisch for constructive discussion. This material is based upon the work supported by the U.S. Department of Energy Office of Fusion Energy Sciences under Contracts No. DE-SC0016253 and No. DE-SC0019135, the Department of Energy National Nuclear Security Administration under Award No. DE-NA0001944, the National Science Foundation under Contract No. PHY-1705224, the University of Rochester, and the New York State Energy Research and Development Authority.

[1] T. Südmeyer, S. V. Marchese, S. Hashimoto, C. R. E. Baer, G. Gingras, B. Witzel, and U. Keller, Femtosecond laser oscillators for high-field science, Nat. Photonics **2**, 599 (2008).

[2] I. Adamovich *et al.*, *Plasma: At the Frontier of Scientific Discovery* (DOE SC & OFES, Washington, DC, 2016).

[3] X. Liu, D. Du, and G. Mourou, Laser ablation and micromachining with ultrashort laser pulses, IEEE J. Sel. Top. Quantum Electron. **33**, 1706 (1997).

[4] I. Kuznetsov, J. Filevich, F. Dong, M. Woolston, W. Chao, E. Anderson, E. R. Bernstein, D. C. Crick, J. J. Rocca, and C. S. Menoni, Three-dimensional nanoscale molecular imaging by extreme ultraviolet laser ablation mass spectrometry, Nat. Commun. **6**, 6944 (2015).

[5] M. A. Klosner, H. A. Bender, W. T. Silfvast, and J. J. Rocca, Intense plasma discharge source at 13.5 nm for extreme-ultraviolet lithography, Opt. Lett. **22**, 34 (1997).

[6] M. Bauer, C. Lei, K. Read, R. Tobey, J. Gland, M. M. Murnane, and H. C. Kapteyn, Direct Observation of Surface Chemistry Using Ultrafast Soft-X-Ray Pulses, Phys. Rev. Lett. **87**, 025501 (2001).

[7] E. Goulielmakis, Z.-H. Loh, A. Wirth, R. Santra, N. Rohringer, V. S. Yakovlev, S. Zherebtsov, T. Pfeifer, A. M. Azzeer, M. F. Kling, S. R. Leone, and F. Krausz, Real-time observation of valence electron motion, Nature (London) **466**, 739 (2010).

[8] P. Jaeglé, *Coherent Sources of XUV Radiation* (Springer, New York, 2006).

[9] S. E. Harris, J. F. Young, A. H. Kung, D. M. Bloom, and G. C. Bjorklund, Generation of Ultraviolet and Vacuum Ultraviolet Radiation, edited by R. G. Brewer and A. Mooradian, *Laser Spectroscopy* (Springer, Boston, 1974).

[10] P. M. Paul, E. S. Toma, P. Breger, G. Mullot, F. Augé, Ph. Balcou, H. G. Muller, and P. Agostini, Observation of a train of attosecond pulses from high harmonic generation, Science **292**, 1689 (2001).

[11] P. Agostini and L. F. DiMauro, The physics of attosecond light pulses, Rep. Prog. Phys. **67**, 813 (2004).

[12] A. McPherson, G. Gibson, H. Jara, U. Johann, T. S. Luk, I. A. McIntyre, K. Boyer, and C. K. Rhodes, Studies of multiphoton production of vacuum-ultraviolet radiation in the rare gases, J. Opt. Soc. Am. B **4**, 595 (1987).

[13] S. C. Wilks, J. M. Dawson, W. B. Mori, T. Katsouleas, and M. E. Jones, Photon Accelerator, Phys. Rev. Lett. **62**, 2600 (1989).

[14] J. T. Mendonça, *Theory of Photon Acceleration* (Institute of Physics Publishing, Bristol, 2001).

[15] E. Esarey, G. Joyce, and P. Sprangle, Frequency up-shifting of laser pulses by copropagating ionization fronts, Phys. Rev. A **44**, 3908 (1991).

[16] L. O. Silva and J. T. Mendonça, Photon acceleration in superluminous and accelerated ionization fronts, IEEE Trans. Plasma Sci. **24**, 316 (1996).

[17] R. L. Savage Jr., C. Joshi, and W. B. Mori, Frequency Upconversion of Electromagnetic Radiation upon Transmission into an Ionization Front, Phys. Rev. Lett. **68**, 946 (1992).

[18] W. M. Wood, C. W. Siders, and M. C. Downer, Femtosecond growth dynamics of an underdense ionization front measured by spectral blueshifting, IEEE Trans. Plasma Sci. **21**, 20 (1993).

[19] J. M. Dias, C. Stenz, N. Lopes, X. Badiche, F. Blasco, A. Dos Santos, L. Oliveira e Silva, A. Mysyrowicz, A. Antonetti, and J. T. Mendonça, Experimental Evidence of Photon Acceleration of Ultrashort Laser Pulses in

Relativistc Ionization Fronts, Phys. Rev. Lett. **78**, 4773 (1997).

[20] J. M. Dias, L. Oliveira e Silva, and J. T. Mendonça, Photon acceleration versus frequency-domain interferometry for laser wakefield diagnostics, Phys. Rev. ST Accel. Beams **1**, 031301 (1998).

[21] J. M. Dias, N. C. Lopes, L. O. Silva, G. Figueira, J. T. Mendonça, C. Stenz, F. Blasco, A. Dos Santos, and A. Mysyrowicz, Photon acceleration of ultrashort laser pulses by relativistic ionization fronts, Phys. Rev. E **66**, 056406 (2002).

[22] M. Lampe, E. Ott, and J. H. Walker, Interaction of electromagnetic waves with a moving ionization front, Phys. Fluids **21**, 42 (1978).

[23] S. C. Wilks, J. M. Dawson, and W. B. Mori, Frequency Up-Conversion of Electromagnetic Radiation with Use of an Overdense Plasma, Phys. Rev. Lett. **61**, 337 (1988).

[24] M. R. Edwards, K. Qu, Q. Jia, J. M. Mikhailova, and N. J. Fisch, Cascaded chirped photon acceleration for efficient frequency conversion, Phys. Plasmas **25**, 053102 (2018).

[25] N. C. Lopes, G. Figueira, J. M. Dias, L. O. Silva, J. T. Mendonça, Ph. Balcou, G. Rey, and C. Stenz, Laser pulse frequency up-shifts by relativistic ionization fronts, Europhys. Lett. **66**, 371 (2004).

[26] D. H. Froula, D. Turnbull, A. S. Davies, T. J. Kessler, D. Haberberger, J. P. Palastro, S.-W. Bahk, I. A. Begishev, R. Boni, S. Bucht, J. Katz, and J. L. Shaw, Spatiotemporal control of laser intensity, Nat. Photonics **12**, 262 (2018).

[27] A. Sainte-Marie, O. Gobert, and F. Quéré, Controlling the velocity of ultrashort light pulses in vacuum through spatio-temporal couplings, Optica **4**, 1298 (2017).

[28] C. G. Durfee III and H. M. Milchberg, Light Pipe for High Intensity Laser Pulses, Phys. Rev. Lett. **71**, 2409 (1993).

[29] H. M. Milchberg, T. R. Clark, C. G. Durfee III, and T. M. Antonsen, Development and applications of a plasma waveguide for intense laser pulses, Phys. Plasmas **3**, 2149 (1996).

[30] D. Kaganovich, J. P. Palastro, Y.-H. Chen, D. F. Gordon, M. H. Helle, and A. Ting, Simulation of free-space optical guiding structure based on colliding gas flows, Appl. Opt. **54**, F144 (2015).

[31] J. P. Palastro, D. Turnbull, S.-W. Bahk, R. K. Follett, J. L. Shaw, D. Haberberger, J. Bromage, and D. H. Froula, Ionization waves of arbitrary velocity driven by a flying focus, Phys. Rev. A **97**, 033835 (2018).

[32] D. Turnbull, P. Franke, J. Katz, J. P. Palastro, I. A. Begishev, R. Boni, J. Bromage, A. L. Milder, J. L. Shaw, and D. H. Froula, Ionization Waves of Arbitrary Velocity, Phys. Rev. Lett. **120**, 225001 (2018).

[33] M. Aoyama, T. Harimoto, J. Ma, Y. Akahane, and K. Yamakawa, Second-harmonic generation of ultra-high intensity femtosecond pulses with a KDP crystal, Opt. Express **9**, 579 (2001).